Commun. Comput. Phys.
doi: 10.4208/cicp.190511.111111a

Vol. **12**, No. 4, pp. 1129-1147
October 2012

Dynamic Modeling of Phase Crossings in Two-Phase Flow

S. Madsen*, C. Veje and M. Willatzen

Alsion 2, Mads Clausen Institute, University of Southern Denmark, DK-6400 Sønderborg, Denmark.

Received 19 May 2011; Accepted (in revised version) 11 November 2011

Available online 17 April 2012

Abstract. Two-phase flow and heat transfer, such as boiling and condensing flows, are complicated physical phenomena that generally prohibit an exact solution and even pose severe challenges for numerical approaches. If numerical solution time is also an issue the challenge increases even further. We present here a numerical implementation and novel study of a fully distributed dynamic one-dimensional model of two-phase flow in a tube, including pressure drop, heat transfer, and variations in tube cross-section. The model is based on a homogeneous formulation of the governing equations, discretized by a high resolution finite difference scheme due to Kurganov and Tadmore.

The homogeneous formulation requires a set of thermodynamic relations to cover the entire range from liquid to gas state. This leads a number of numerical challenges since these relations introduce discontinuities in the derivative of the variables and are usually very slow to evaluate. To overcome these challenges, we use an interpolation scheme with local refinement.

The simulations show that the method handles crossing of the saturation lines for both liquid to two-phase and two-phase to gas regions. Furthermore, a novel result obtained in this work, the method is stable towards dynamic transitions of the inlet/outlet boundaries across the saturation lines. Results for these cases are presented along with a numerical demonstration of conservation of mass under dynamically varying boundary conditions. Finally we present results for the stability of the code in a case of a tube with a narrow section.

AMS subject classifications: 76T10, 80A20, 65M06

Key words: Two-phase flow, heat exchange, flow boiling, central difference.

1 Introduction

Simulation of two-phase flow and heat transfer is important for the analysis of a range of fundamental physical processes and phenomena such as evaporation and condensa-

*Corresponding author. *Email addresses:* sma@mci.sdu.dk (S. Madsen), veje@mci.sdu.dk (C. Veje), willatzen@mci.sdu.dk (M. Willatzen)

tion. Thus, the application of numerical methods has a substantial impact on research and development within a large range of industrial applications, for example, the design of heat exchangers in areas of power generation, refrigeration and air conditioning, industrial thermal- and chemical process plants. As the requirements of these industrial applications tend towards increasing energy efficiency, the requirements for model accuracy and stability of the numerical tools increase. Consequently there is a growing need for more detail in the modeling of the basic phenomena while at the same time keeping the computation efficient.

Computationally demanding components in the systems mentioned above are mainly the dry-expansion evaporators in refrigeration and air-conditioning systems. Lumped component models for these components are traditionally solved using NTU-ϵ - methods or models of the moving boundary type [1–4]. Such models have an advantage by realistically demonstrating dynamical behavior of the component in relation to capacities, temperature, and pressure levels although formulated as lumped models. A disadvantage is a loss of detail in the modeling and the handling of fluid-zone switching which may result in numerical instability and increased computation time.

In a general effort to investigate the dynamic behavior of two-phase flow and heat transfer we are seeking a mathematical formulation that provides a stable numerical solution despite the problem involves a dynamically changing number of fluid zones [5]. Several works have been published on fully distributed models solving the governing equations [6–9]. However, the fast pressure dynamics of the full set of governing equations is neglected in earlier analyses in order to accomplish faster computation times and numerically stable codes. Also, these earlier models are generally limited to constant cross sectional area of the tubes

To handle the above difficulties, high resolution difference schemes have been developed as "black box" solvers for both conservation laws and Hamilton-Jacobi equations [10, 11]. In the semi-discrete form, they are easily implemented using, e.g., Runge-Kutta methods for ordinary differential equations, and therefore an attractive alternative to commercial CFD codes. Applications of high resolution difference schemes to two-phase flow problems include the so-called separated models where liquid and gas are treated as two separate fluids [12]. In these models, interphase exchange terms are needed to model the evaporation/condensation process and the form of the terms depends on the two-phase flow regime [13]. In the homogenous formulation, these details are instead included in the thermodynamic relations available from, for example, the National Institute of Standards and Technology [14].

In this paper, we develop a novel numerical model to effectively handle the fast dynamics and the associated phenomena when crossing the phase boundaries. We present the application of the Kurganov-Tadmor (KT) semi discrete central difference method [10, 11] to the case of two-phase boiling flow in a single tube exchanging heat with the surroundings. The model is derived for a tube of arbitrary cross section.

2 Formulation of one-dimensional governing equations

Modeling of two-phase fluid flow is traditionally cast in the framework of a homogeneous or a separated flow formulation. In the separated formulation each phase is treated separately and two sets of conservation equations are set up for the problem. Evaporation and condensation are then treated as sink and source terms, respectively. The homogeneous formulation seeks to treat the flow as a single fluid and introduces a variable x that represents the local quality of one of the phases. The thermodynamics of the phase transition is thus accounted for through this variable as specified by the equation of state. In this paper we will apply the homogenous formulation such as described in various text books [13, 15].

The equations describing mass- and momentum conservation (the Navier-Stokes equations), and the fluid energy equation form the basis of our formulation. They can be written as

$$\frac{\partial \rho}{\partial t}+\nabla\cdot(\rho\mathbf{v})=0, \tag{2.1}$$

$$\frac{\partial \mathbf{v}}{\partial t}+(\mathbf{v}\cdot\nabla)\,\mathbf{v}=-\frac{1}{\rho}\nabla P+\frac{1}{\rho}\nabla\sigma', \tag{2.2}$$

$$\rho\left(\frac{\partial h}{\partial t}+\mathbf{v}\cdot\nabla h\right)-\frac{\partial P}{\partial t}-\mathbf{v}\cdot\nabla P=q', \tag{2.3}$$

where ρ, P, h, $\mathbf{v}$, q', σ, ∇, and t are the fluid mass density, pressure, fluid specific enthalpy, fluid velocity, boundary heat flux, the viscous stress tensor, the nabla operator referring to spatial derivatives, and time, respectively. Apparently, since the governing equations are formulated mathematically in "strong" form in the homogeneous formulation, caution must be taken as to whether all variables including thermodynamic parameters are indeed differentiable everywhere in the solution space. This is, however, not the case when phase changes take place as they do in a boiling flow. In the homogeneous formulation used in this work (refer to later discussions), we have made a specific choice in circumventing this problem for, e.g., the speed of sound and other thermodynamic derivatives which are not differentiable exactly when phase changes occur. In a future work, emphasis will be given to the accuracy of different choices in treating non-differentiable quantities using the homogeneous formulation.

We seek to derive a set of dynamic one-dimensional spatial differential equations, yet maintaining the possibility to address geometries of varying cross sectional area along the spatial coordinate z, as shown in Fig. 1. This is done by integration of Eqs. (2.1)-(2.3) over the local cross sectional area $A(z)$. We apply the following operator

$$\int_{A(z)} dA=\int_0^{2\pi}\int_0^{R(z,\theta)} r dr d\theta, \tag{2.4}$$

to each term in the three equations (using cylindrical coordinates (z,r,θ)) where $R(z,\theta)$ is

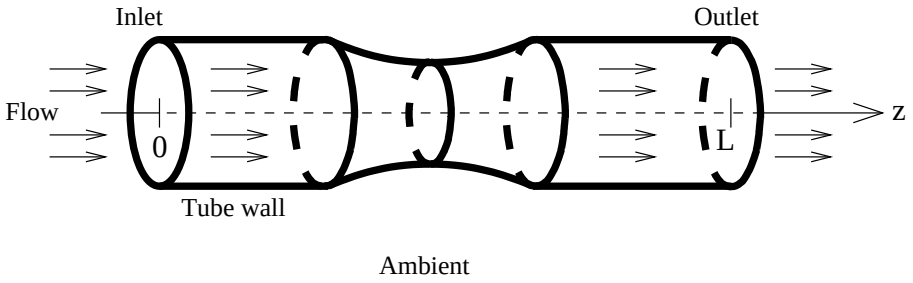

Figure 1: Schematic view of the geometry and flow direction. The fluid is interacting with the ambient through the walls.

the radial extend of the geometry. If a term does not depend on the radial coordinate r and angle θ, this operator corresponds to multiplication by $A(z)$.

We consider all thermodynamic properties to be a function of z and t but independent of r and θ, i.e.

$$\rho=\rho(z,t), \tag{2.5a}$$
$$P=P(z,t), \tag{2.5b}$$
$$T=T(z,t), \tag{2.5c}$$
$$h=h(z,t), \tag{2.5d}$$
$$T_W=T_W(z,t), \tag{2.5e}$$

and assume the fluid velocity to be along the z direction and a function of all four variables,

$$\mathbf{v}=(v_z(z,r,\theta,t),0,0), \tag{2.6}$$

valid for small $|dA/dz|$.

We also assume that the flow velocity vanishes at the tube wall due to small viscous effects, i.e.

$$v_z(z,R(z,\theta),\theta,t)=0, \tag{2.7}$$

and we introduced the average quantity $\langle f\rangle$ defined by

$$\langle f\rangle=\frac{1}{A(z)}\int_{A(z)} f dA. \tag{2.8}$$

Upon acting with the operator in Eq. (2.4), Eqs. (2.1)-(2.3) become

$$\frac{\partial\rho}{\partial t}A(z)+\frac{\partial[\langle v_z\rangle\rho A(z)]}{\partial z}=0, \tag{2.9}$$
$$\frac{\partial\langle v_z\rangle}{\partial t}A(z)+\frac{1}{2}\frac{\partial}{\partial z}\left[\langle v_z^2\rangle A(z)\right]=-\frac{1}{\rho}\frac{\partial P}{\partial z}A(z)-\frac{A(z)}{\rho}\left(\frac{\partial P}{\partial z}\right)_{fric}, \tag{2.10}$$
$$\rho\frac{\partial h}{\partial t}-\frac{\partial P}{\partial t}+\rho\frac{\partial h}{\partial z}\langle v_z\rangle-\frac{\partial P}{\partial z}\langle v_z\rangle=\frac{4}{D}\alpha(T_W-T), \tag{2.11}$$

where the right hand side term in Eq. (2.11) expresses the boundary heat flux where T_W, T, α, D, are the wall temperature, fluid temperature, heat-transfer coefficient accounting for the combined effect of conduction, convection, and radiation and inner wall diameter respectively. The viscous stress tensor term is approximated by a pressure loss term along the z coordinate, and

$$A(z)=\frac{\pi}{4}D^2(z). \tag{2.12}$$

For a flat turbulent flow profile where the flow velocity v_z is equal to the average flow velocity $\langle v_z\rangle$ everywhere as a function of r except very near the wall (i.e., in the boundary layer where v_z drops to zero fast as r approaches $R(z,\theta)$), we have

$$\langle v_z^2\rangle=\langle v_z\rangle^2. \tag{2.13}$$

However, for a laminar parabolic flow profile,

$$v_z(r)=2\langle v_z\rangle\left(1-\frac{r^2}{R^2(z)}\right), \tag{2.14}$$

one finds

$$\langle v_z^2\rangle=\frac{4}{3}\langle v_z\rangle^2. \tag{2.15}$$

If needed, a local assessment in the modeling as to whether flow is turbulent or laminar can be invoked and then use a relation on the form $\langle v_z^2\rangle=f(Re)\langle v_z\rangle^2$, where Re is the local Reynolds number. $f=1$ gives Eq. (2.13) and $f=4/3$ gives Eq. (2.15). In the rest of this paper we assume a turbulent flow profile and set $\langle v_z^2\rangle=\langle v_z\rangle^2$.

With the above expressions, we finally have three differential equations in three unknowns: $\langle v_z\rangle$,ρ, and h that, together with the wall temperature equation (for T_W), complete the equation framework for a geometry of varying cross sectional area. Recasting the above set of differential equations in terms of the mass flow defined by

$$\dot{m}(z,t)=\rho A(z)\langle v_z\rangle, \tag{2.16}$$

the governing equations formulated in terms of density, mass flow, enthalpy together with an energy equation for the wall then become

$$\frac{\partial(\rho A)}{\partial t}+\frac{\partial\dot{m}}{\partial z}=0, \tag{2.17}$$

$$\frac{\partial\dot{m}}{\partial t}+\frac{\partial}{\partial z}\left(\frac{\dot{m}^2}{\rho A}\right)+\frac{\dot{m}^2}{2\rho A^2}\frac{\partial A}{\partial z}=-A\frac{\partial P}{\partial z}-A\left(\frac{\partial P}{\partial z}\right)_{fric}, \tag{2.18}$$

$$\rho\frac{\partial h}{\partial t}-\frac{\partial P}{\partial t}+\frac{\dot{m}}{A}\frac{\partial h}{\partial z}-\frac{\dot{m}}{\rho A}\frac{\partial P}{\partial z}=\frac{4}{D}\alpha(T_W-T), \tag{2.19}$$

$$(C_W\rho_W A_W)\frac{\partial T_W}{\partial t}=\alpha\pi D(T-T_W)+\alpha_o\pi D_o(T_A-T_W)+\lambda_W A_W\frac{\partial^2 T_W}{\partial z^2}, \tag{2.20}$$

where C_W, ρ_W, A_W, α_o, D_o, T_A, and λ_W denote the wall heat capacity, wall mass density, wall cross-sectional area, heat-transfer coefficient to the ambient, outer wall diameter, ambient temperature, and the wall heat conductivity, respectively. Note that D_o, A_W, D, and A generally are functions of the axial coordinate z and allows us to approximate different 3D geometries as variations along the z direction in the inner and outer cross sectional areas.

Eqs. (2.17)-(2.20) must be supplemented with boundary conditions. We use the following

$$\dot{m}(0,t) = \dot{m}_{in}(t), \tag{2.21}$$

$$h(0,t) = h_{in}(t), \tag{2.22}$$

$$\dot{m}(L,t) = \rho(L,t)\dot{V}(t), \tag{2.23}$$

$$\left.\frac{\partial T_W}{\partial z}\right|_{z=0,L} = 0, \tag{2.24}$$

for a geometry starting at $z=0$ and ending at $z=L$. $\dot{V}$ is the volume flow out of the system. These boundary conditions are common if Eqs. (2.17)-(2.20) models for example flow boiling in a tube, with an outlet condition determined by a positive displacement machine such as, e.g., a compressor. If the process is condensing flow, the volume flow boundary condition is usually replaced by a mass flow boundary condition, e.g. $\dot{m}(L,t) = \dot{m}_{out}$.

3 Thermodynamics

Thermodynamic functions, such as P and T, must be supplied in order to do calculations with Eqs. (2.17)-(2.20). These are assumed to be functions of the dependent variables ρ and h, e.g. $P = P(h,\rho)$ and then

$$\frac{\partial P}{\partial t} = \frac{\partial P}{\partial h}\frac{\partial h}{\partial t} + \frac{\partial P}{\partial \rho}\frac{\partial \rho}{\partial t} = \frac{\partial P}{\partial h}\frac{\partial h}{\partial t} - \frac{1}{A}\frac{\partial P}{\partial \rho}\frac{\partial \dot{m}}{\partial z}. \tag{3.1}$$

This relation is used in Eqs. (2.17)-(2.20) to eliminate the time-derivatives of the pressure. Notice that we are treating the flow in a homogeneous formulation so that the two-phase nature of the underlying thermodynamics are expressed in terms of the saturated quantities and the vapor quality. For the density this means:

$$\rho = \left(\frac{x}{\rho_g} + \frac{1-x}{\rho_l}\right)^{-1}, \tag{3.2}$$

where subscript g and l refers to saturation values of gas and liquid phase, respectively. For simplicity, each phase is assumed to propagate with the same velocity, although a slip-relation could have been included [13].

In addition, the heat transfer coefficient, α, and the pressure loss term due to friction, $(\partial P/\partial z)_{fric}$, must be calculated. For two-phase flow in particular the pressure drop due to acceleration (rapidly decreasing density) usually dominates over the frictional pressure drop. Numerous correlations for two-phase flow pressure drops can be found in the literature [13]. For the sake of simplicity, we use the conventional expression applied to the two-phase region

$$\left(\frac{\partial P}{\partial z}\right)_{fric} = 4f\frac{1}{D}\frac{\dot{m}^2}{\rho A^2}, \tag{3.3}$$

where f is the Fanning friction factor here given by the Blasius correlation

$$f = 0.079Re^{-0.25}. \tag{3.4}$$

The Reynolds number is

$$Re = \frac{|\dot{m}|D}{\mu A}, \tag{3.5}$$

with the viscosity, μ, depending on the local vapor quality $x = x(h,P)$ as

$$\mu = \left(\frac{x}{\mu_g} + \frac{1-x}{\mu_l}\right)^{-1}, \tag{3.6}$$

where μ_g and μ_l refer to the viscosity in the gas phase and liquid phase, respectively.

For the heat transfer coefficient numerous correlations [16] exist but again for simplicity we apply a linear interpolation between the liquid and gas phases, i.e.,

$$\alpha = (1-x)\alpha_l + x\alpha_g, \tag{3.7}$$

with

$$\alpha_k = \frac{Nu_k\lambda_k}{D}, \tag{3.8}$$

where the subscript 'k' is used to designate either 'g' (gas) or 'l' (liquid). α_k is the single-phase heat transfer coefficient. $\lambda_k = \lambda_k(P)$ is the thermal conductivity and Nu_k is the Nusselt number given by the Dittus-Boelter equation

$$Nu_k = 0.023Re_k^{0.8}Pr_k^{0.3}, \tag{3.9}$$

$$Re_k = \frac{|\dot{m}|D}{\mu_k A}, \tag{3.10}$$

$$Pr_k = \frac{\mu_k C_{p,k}}{\lambda_k}, \tag{3.11}$$

where $C_{p,k}=C_{p,k}(P)$ is the specific heat, $\mu_k=\mu_k(P)$ is the dynamic viscosity, Re_k is the Reynolds number, and Pr_k is the Prandtl number.

The remaining thermodynamic functions must be obtained in a different way. We use REFPROP [14], which, for many different fluids, implements a highly accurate equation of state used to calculate thermodynamic quantities. The pressure is determined from ρ and h and then the remaining functions are determined from P and/or h.

For many thermodynamic quantities, REFPROP employs an iterative approach. This process can be very time consuming, especially near phase transitions. To speed this part up, we pre-calculate tables for the needed thermodynamic functions and use interpolation between the grid points. Our numerical experiments indicate that accurate determination of $P(h,\rho)$ are of utmost importance for both accuracy and stability. To determine $P(h,\rho)$ we use the monotone piecewise bicubic interpolation of Carlson and Fritsch [17] on a recursively subdivided grid. To generate the grid, we start with an initial grid of 800x800 points. At grid centers and centers of grid lines, the interpolated function is compared to the value obtained from REFPROP. If the relative error is larger than 10^{-3}, we subdivide the grid cell by a factor of 4. This is done recursively until the interpolated function matches REFPROP within the relative accuracy. When we subdivide a grid cell, we break the continuity of the bicubic interpolation along the boundaries of the subdivided cell. However, since we demand all interpolated cells to be very close to the "true" value, the possible discontinuities along the cell lines become, in practice, very small and does not provide a problem.

The characteristic velocities of Eqs. (2.17)-(2.19) can be estimated by assuming $\alpha=(\partial P)/(\partial z)_{fric}=0$, inserting a harmonic wave of the form $Ae^{i(kz-\omega t)}$ for each dependent variable in the equations of motion, and solve the resulting eigenvalue problem to obtain $v=\omega/k$. The result is

$$v_0=\frac{\dot{m}}{A\rho}, \tag{3.12}$$

$$v_\pm=v_0\pm\sqrt{\frac{\rho\frac{\partial P}{\partial\rho}}{\rho-\frac{\partial P}{\partial h}}}\equiv v_0\pm c. \tag{3.13}$$

The velocity v_0 is recognised as the mass-flow velocity and $v_\pm$ are the mass-flow velocity plus or minus the speed of sound, c.

The partial derivatives of the pressure are calculated using finite differences from gridded $\rho(h,P)$ data and then using relations

$$\frac{\partial P}{\partial\rho}=1\Big/\frac{\partial\rho}{\partial P}, \tag{3.14}$$

$$\frac{\partial P}{\partial h}=-\frac{\partial\rho}{\partial h}\Big/\frac{\partial\rho}{\partial P}, \tag{3.15}$$

that follows from inserting the differential expression

$$d\rho = \frac{\partial P}{\partial p} dp + \frac{\partial P}{\partial h} dh, \tag{3.16}$$

in the right-hand side of

$$dp = \frac{\partial P}{\partial \rho} d\rho + \frac{\partial P}{\partial h} dh, \tag{3.17}$$

and requiring the resulting left- and right-hand expressions to be identical for any variation of thermodynamic quantities.

Using these relations, the speed of sound can also be expressed as

$$c = \sqrt{\frac{\rho}{\rho \frac{\partial \rho}{\partial P} + \frac{\partial \rho}{\partial h}}}, \tag{3.18}$$

hence

$$\rho \frac{\partial \rho}{\partial P} + \frac{\partial \rho}{\partial h} > 0, \tag{3.19}$$

must be true at all (h,P) since $\rho > 0$.

We use 2nd order central finite differences to obtain $\partial\rho/\partial P$ and $\partial\rho/\partial h$ from $\rho(h,P)$ except at discontinuities (occurring due to phase transitions). At the discontinuities we resort to first order one-sided differences, chosen such that Eq. (3.19) is satisfied at all grid points. The gridded data of partial derivatives are interpolated with bilinear interpolation to guarantee that the inequality (3.19) is satisfied at all (h,ρ).

Fig. 2 shows a plot of the pressure and speed of sound as a function of the density. The pressure is continuous everywhere, while the speed of sound jumps from 6 m/s to 842 m/s at $\rho = 555$ kg/m^3 due to the discontinuous first derivative of the pressure.

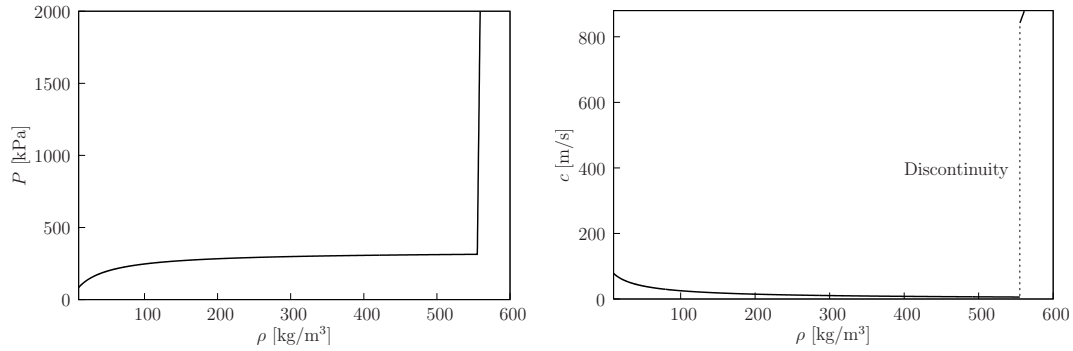

Figure 2: Pressure (left) and speed of sound (right) as a function of ρ for constant $h = 250$ kJ/kg. The pressure is continuous everywhere, while the speed of sound jumps from 6 m/s to 842 m/s at $\rho = 555$ kg/m^3.

4 Central difference scheme

Spatial discretization turns the continuous functions into discrete functions in space. The length of the geometry is discretized using $N+1$ points from $z=0$ to $z=L$, and we will use a lower index as a discrete spatial coordinate, e.g. $f_i=f(i\Delta z,t)$ with $\Delta z=L/N$.

Straight-forward central finite differences applied to Eqs. (2.17)-(2.19) show spurious oscillations which quickly destroy the numerical solution. High resolution central schemes have been developed to avoid such oscillations, to allow possible discontinuities in the solutions, and to be more than first order accurate overall. We have used the KT scheme for conservation laws [11] to discretize Eq. (2.17) and the KT scheme for Hamilton-Jacobi equations [10] to discretize Eqs. (2.18) and (2.19), both in the 2nd order semi-discrete form with characteristic velocities found from Eqs. (3.12) and (3.13). Eq. (2.20) is discretized in space using standard 2nd order central differences, e.g. $f'(i\Delta z,t)\approx(f_{i+1}-f_{i-1})/(2\Delta z)$ where the prime denotes differentiation with respect to z.

To do the time-stepping of the resulting set of ordinary differential equations, we use the 3rd order strong stability preserving Runge-Kutta method [18] with time step

$$\Delta t=C\frac{\Delta z}{v_{\max}}, \tag{4.1}$$

where v_{max} is the maximum characteristic velocity in the tube (from Eqs. (3.12) and (3.13)). C is the Courant number, which is typically taken to be 0.95. However, when going from the two-phase state into the liquid state (or vise-versa), we use a value of 0.24 in order to preserve stability.

4.1 Boundary conditions

The 2nd order KT scheme has a five point spatial stencil. At each boundary, we use two ghost points to implement physical and numerical boundary conditions. For the central 2nd order finite differences used for the temperature, only one ghost point is needed. At the boundaries we use

$$\dot{m}_0=\dot{m}_{in}, \tag{4.2}$$
$$\dot{m}_N=\rho_N\dot{V}, \tag{4.3}$$
$$h_0=h_{in}, \tag{4.4}$$
$$T_{W,-1}=T_{W,1}, \tag{4.5}$$
$$T_{W,N+1}=T_{W,N-1}, \tag{4.6}$$

to implement the physical boundary conditions in Eqs. (2.21)-(2.24).

The missing numerical boundary conditions for the five point stencil of the KT scheme can be constructed using extrapolation. We consider here two forms of extrapolation: The first is just to use the values on the boundary, i.e. (shown for $\dot{m}$ only, ρ and h

are similar)

$$\dot{m}_{-2} = \dot{m}_{-1} = \dot{m}_0, \tag{4.7}$$

and the second is to fit a 2nd order polynomial to the first 3 values, giving

$$\dot{m}_{-1} = 3\dot{m}_0 - 3\dot{m}_1 + \dot{m}_2, \qquad \dot{m}_{-2} = 6\dot{m}_0 - 8\dot{m}_1 + 3\dot{m}_2. \tag{4.8}$$

5 Simulations

We perform simulations on boiling flow in a tube using the parameters given in Table 1 and with R600a (isobutane) as the working fluid [19]. As a starting point, we use the following constant values:

$$\dot{m}(z) = 0.002 \text{ kg/s}, \quad h(z) = 250 \text{ kJ/kg}, \quad \rho(z) = 60 \text{ kg/m}^3, \quad T_w(z) = 300 \text{ K}. \tag{5.1}$$

Table 1: Common parameters and initial data used in the simulations. Working fluid is R600a (isobutane). In Fig. 10, A is changed along the tube and is not the constant value shown here.

Parameter	Value	Unit
L	10	m
C_W	385	J/(kg K)
ρ_W	$8.96 \cdot 10^3$	kg/m^3
A_W	$2.1 \cdot 10^{-5}$	m^2
A	$2.8 \cdot 10^{-5}$	m^2
λ	386	W/(m^{2}K)
T_A	300	K
α_0	100	W/(m^{2}K)
h_{in}	$2.5 \cdot 10^5$	J/kg
$\dot{V}$	$2 \cdot 10^{-4}$	m^3/s

Table 2: The test case is 250 s long and consists of several steps in the inlet mass flow. At $t = 0$ s, the state is given in Eq. (5.1). The 'Figure' column refers to the figure showing the steady state, obtained after 50 s of simulation time.

time [s]	$\dot{m}_{in}$ [kg/s]	Figure
0-50	0.002	4
50-100	0.001	5
100-150	0.002	4
150-200	0.01	6
200-250	0.002	4

We simulate for 250 s and make steps in the mass flow at the inlet according to Table 2. The figure number in the last column shows the state obtained just before doing the next step. These states are very close to steady state. Fig. 3 shows the locations of the

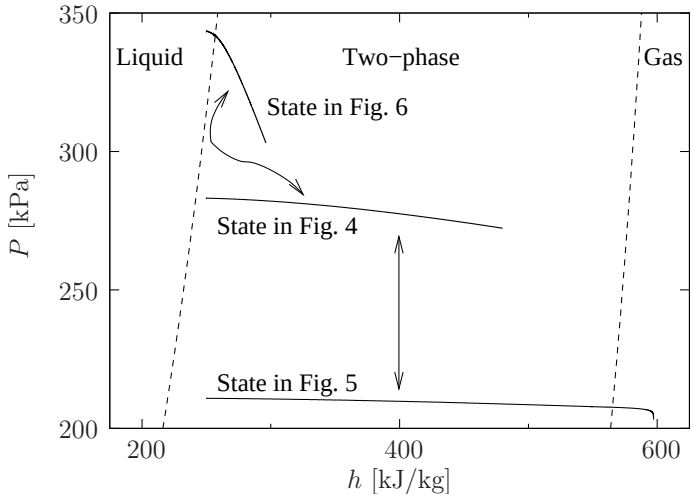

Figure 3: Overview of the test case in a $P-h$ diagram. The arrows schematically show the transient behavior of the tube as the boundary conditions change according to Table 2. The dashed lines marked h_l and h_g show the location of the transitions to the pure liquid and gas phases. The solid lines represent steady-state (h,ρ) values from $z=0$ (leftmost point) to $z=L$ (rightmost point).

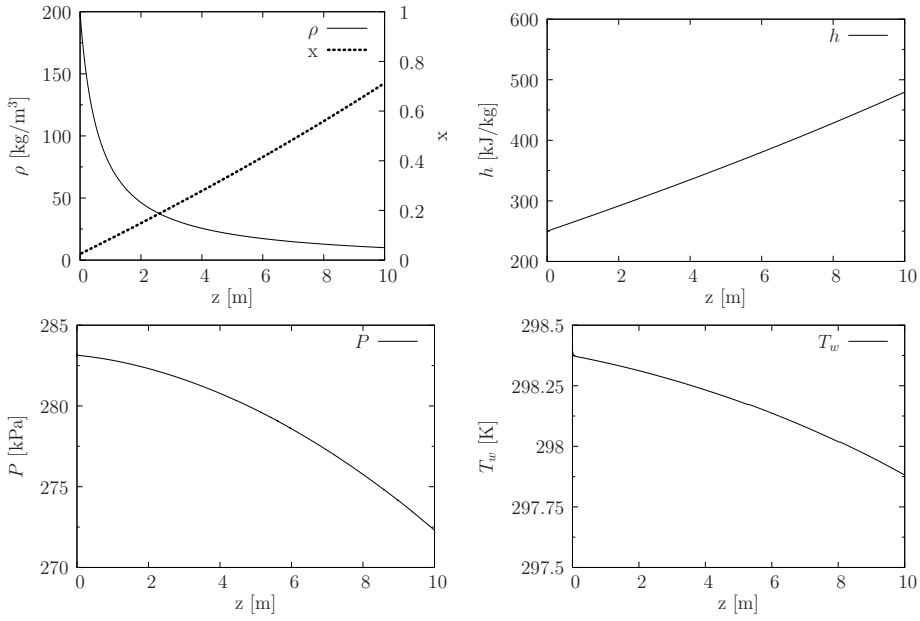

Figure 4: Steady state with $\dot{m}_{in}=0.002$ kg/s.

three different steady states in a $P-h$ diagram. The figure number associated with the simulation results for the three states are also shown in Fig. 3. As seen the first process in Fig. 4 is a pure two-phase flow from inlet to outlet. The next, in Fig. 5, is a conventional process of two-phase inlet and superheated gas outlet. Here the two-phase/gas bound-

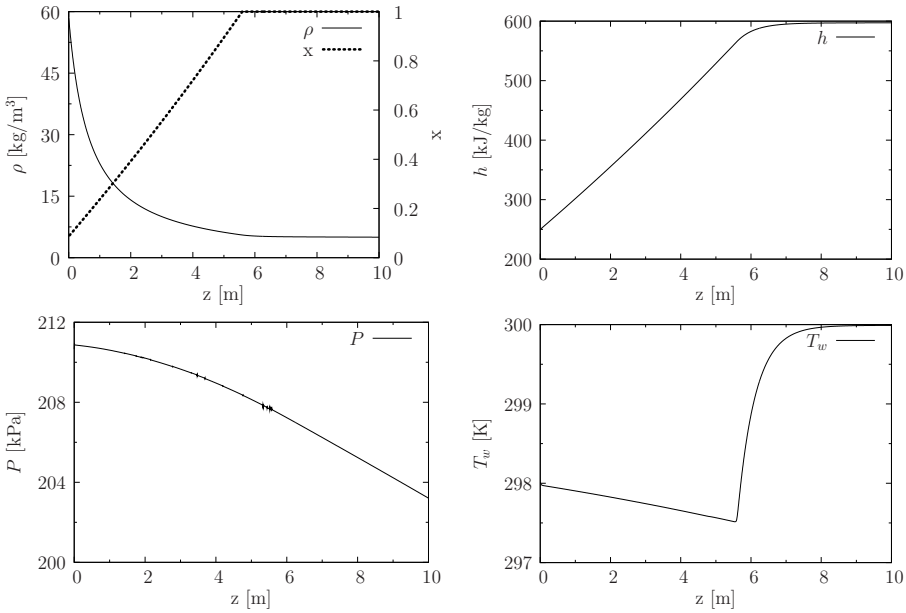

Figure 5: Steady state with $\dot{m}_{in} = 0.001$ kg/s.

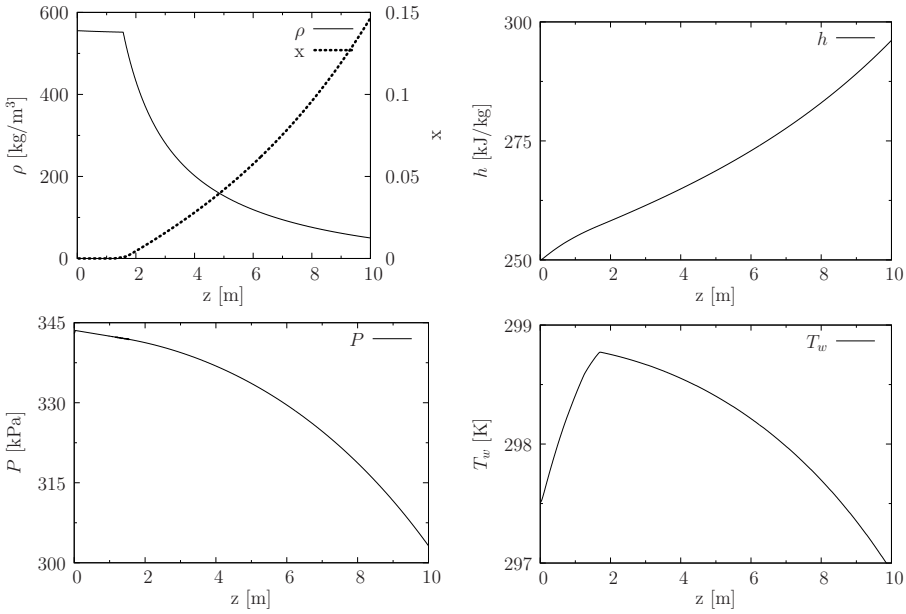

Figure 6: Steady state with $\dot{m}_{in} = 0.01$ kg/s.

ary is crossed. The last, in Fig. 6, is a process crossing the liquid line from sub-cooled liquid into the two-phase region. The system goes from Fig. 4 to Fig. 5 and back again and then from Fig. 4 to Fig. 6 and back again, as indicated by the arrows in Fig. 3.

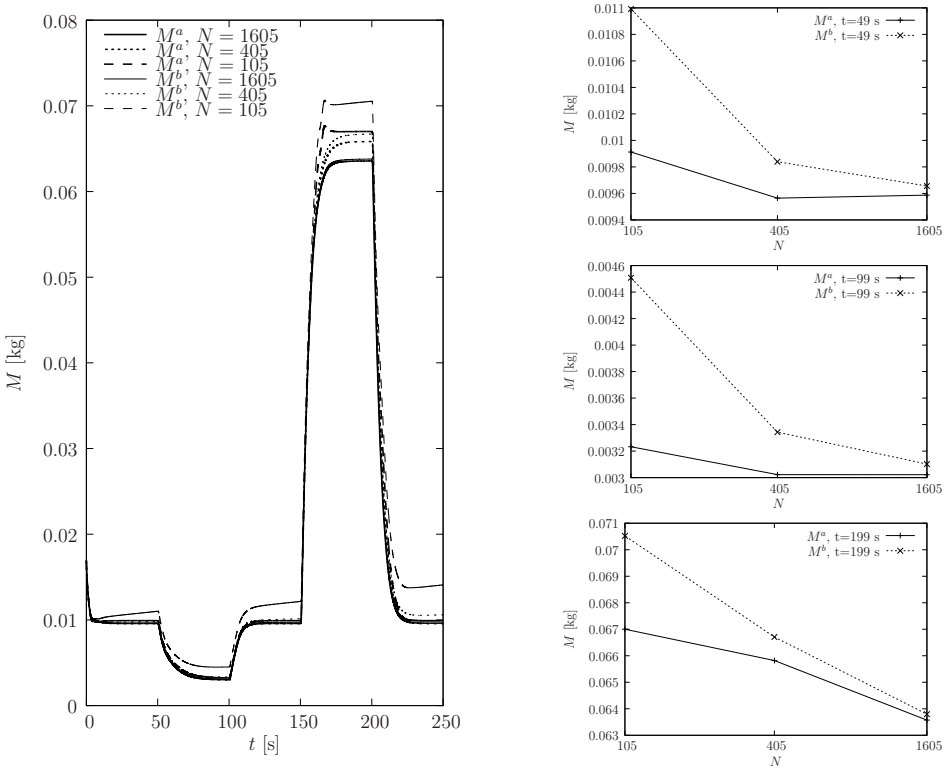

Figure 7: $M^a(t)$ and $M^b(t)$ for the test case with extrapolation by Eqs. (4.7) at both inlet and outlet for different values of N. Values of $M^{a,b}$ corresponding to Figs. 4-6 are shown to the right.

Fig. 4 reflects the overall continuous behavior of the variables. In Fig. 5 we clearly identify the dry-out point associated with the two-phase to gas boundary crossing. This happens at about $z=5.5$ m. In Fig. 6, the point of liquid to two-phase region crossing is also clearly identified at $z=1.8$ m.

To compare different simulations we calculate the total mass of the fluid in the evaporator as

$$M^a(t) = \int_0^L A(z)\rho(z,t)dz, \tag{5.2}$$

$$M^b(t) = M^a(0) + \int_0^t (\dot{m}(0,\tilde{t}) - \dot{m}(L,\tilde{t}))d\tilde{t}. \tag{5.3}$$

The continuity equation requires $M^a(t) = M^b(t)$, which we can use as a measure of accuracy.

The simulation case above was run with the numerical boundary conditions in Eqs. (4.7) and (4.8). However, we found that the 2nd order extrapolation could lead to instabilities when the inlet moves in and/or out of the liquid zone. This is evident from Fig. 6, where the density ρ is seen to have a discontinuous first derivative near $z \sim 1.8$ m.

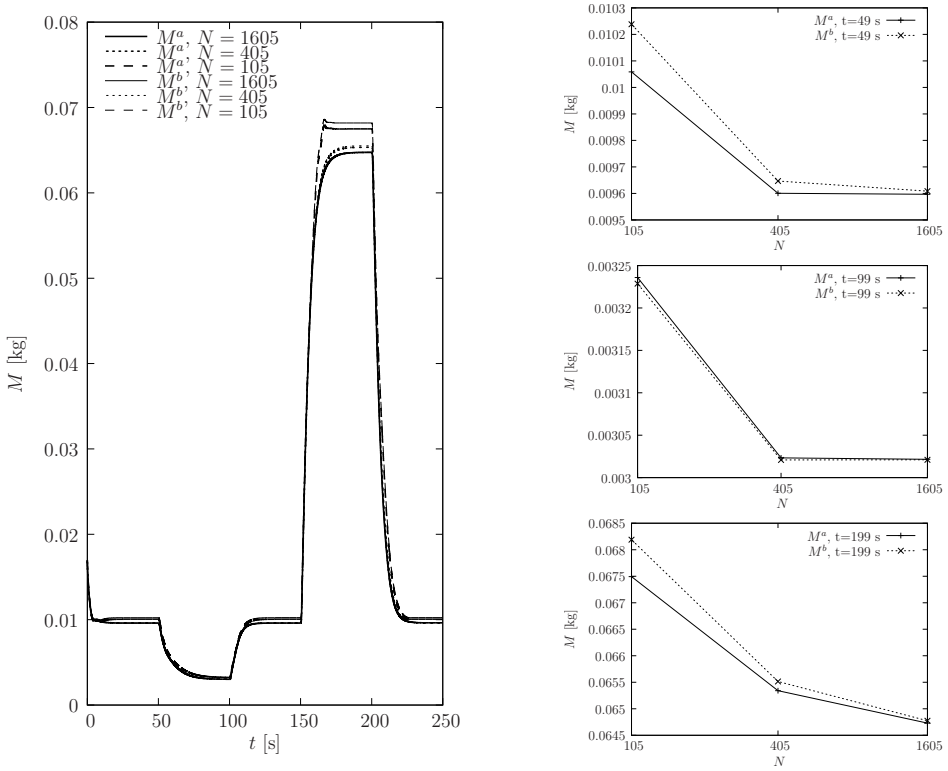

Figure 8: $M^a(t)$ and $M^b(t)$ for the test case with extrapolation by Eqs. (4.7) at both inlet and Eq. 4.8) at the outlet for different values of N. Values of $M^{a,b}$ corresponding to Figs. 4-6 are shown to the right.

This point separates the near constant ρ in the liquid zone and the rapidly changing ρ in the two phase zone. Doing polynomial extrapolation across this point is highly inaccurate, leading to numerical instability and have prevented us from running the test case using Eq. (4.8) at the inlet. We therefore only consider two cases: a) Using Eq. (4.7) at the inlet and outlet and b) Using Eq. (4.7) at the inlet and Eq. (4.8) at the outlet.

In Figs. 7 and 8 we compare these two numerical boundary conditions for different number of discretization points, by calculating $M^a(t)$ and $M^b(t)$. The whole 250 s process indicated in Table 2 is simulated dynamically to underline the stability of the method. The simulation then crosses both saturation lines dynamically and should hereafter return to the initial steady state (e.g. $t=50$ s). The total mass in the tube changes due to the changing boundary conditions. For low discretization ($N=105$) and no extrapolation at the boundary, $M^a(t)$ and $M^b(t)$ are seen to disagree and (more severely), $M^b(t)$ is seen to drift. In the other cases, we get more accurate agreement, and in general the introduction of the 2nd order extrapolation at the outlet increases the consistency.

In steady state one expects $\dot{m}(z)$ to be a constant. In the simulations we do not find this to always be the case, especially for low discretization. In Fig. 9 we compare $\dot{m}$ corresponding to the steady states in Figs. 4-6 for different number of discretization points

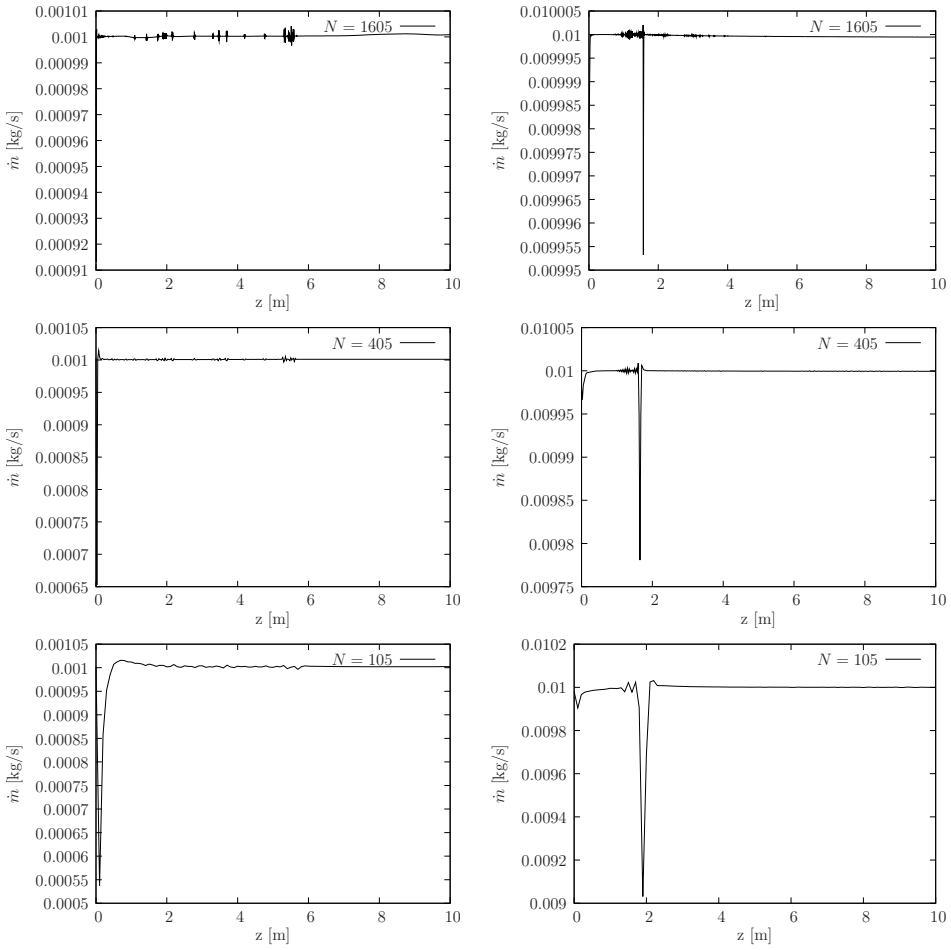

Figure 9: $\dot{m}$ for different N in situations corresponding to Figs. 5 (left) and 6 (right). The height of the sudden jump in mass flow is related to the range shown of the y-axis.

using constant numerical boundary conditions at the inlet and the 2nd order extrapolation at the outlet. Near the inlet we see a sudden jump in $\dot{m}$ when the inlet is two-phase (left column of Fig. 9). This is due to the constant ghost points. If we use the 2nd order extrapolation at the inlet, this jump is greatly reduced. When the inlet is liquid (right column of Fig. 9), the jump in $\dot{m}$ near the inlet is almost gone, since the method of giving ghost points a constant value equal to the first point (or last point) nearly corresponds to using a higher-order extrapolation. However, near the phase change we see a new jump in $\dot{m}$. Fortunately, all these jumps are seen to decrease with better discretization and for the calculations of the total mass in the evaporator (Figs. 7 and 8), these jumps do not seem to be a major problem.

To conclude this section, we show in Fig. 10 a simulation with a pipe with changing cross sectional area. In the middle of the pipe, the radius is changed from 0.003 m to

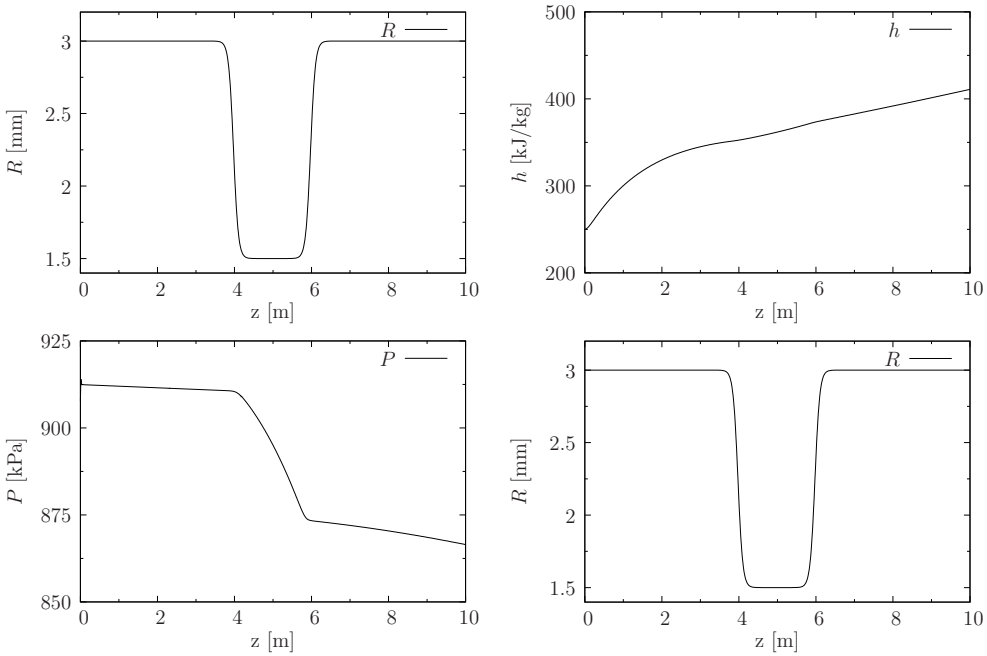

Figure 10: An example of a simulation with a narrowing of the pipe. The lower right plot shows the radius of the pipe. $\dot{m} = 0.006$ kg/s.

0.0015 m and back to 0.003 m again. Liquid is entering the pipe, and as the pressure drops rapidly due to the constriction, the liquid flashes into two phase flow. The stability of the scheme towards such area changes is important for further investigations into, e.g., flashing phenomena in expansion valves.

6 Computational time

The program has been parallelized using the OpenMP implementation in gcc 4.4.4. This is straightforward to do, since the KT scheme combined with the Runge-Kutta time stepping essentially corresponds to a sequence of loops over the grid. The expected complexity of the algorithm is $\mathcal{O}(N^2)$ for fixed length, but the constant of proportionality depends on the speed of sound. The speed of sound in the liquid phase of R600a is typically about 800 m/s and in the gas phase it is typically about 200 m/s. These properties makes simulations including a liquid phase about a factor of 4 slower than simulations including only two-phase and gas.

Fig. 11 shows measurements of the simulation time on a dual quad-core 2.27 GHz Xeon computer. Hyper-threading (doubling the number of cores available to the operating system) was enabled and we tested the program with up to 16 threads, though the computer only contains 8 actual computation cores. The speed-up is the single-thread running time divided by the multi-thread running time. For a small number of points,

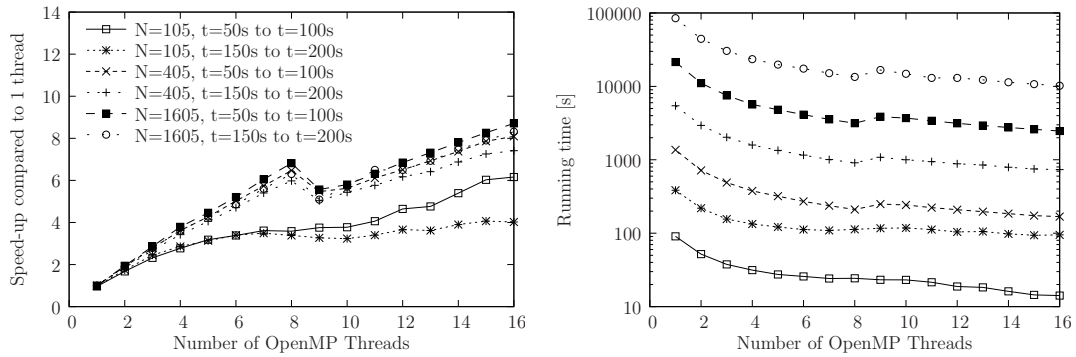

Figure 11: Computational time (right) and speed-up (left) for simulations from t=50s to t=100s (two-phase and gas) and t=150s to t=200s (liquid and two-phase) from Table 2.

the parallel performance of the program is not very good, but for $N \geq 405$, we see a nice linear scaling with the number of threads and a slope slightly below 1. The figure also shows the expected 4-fold difference between two-phase+gas simulations and liquid+two-phase simulations.

7 Conclusion

We have presented transient numerical solutions of the one dimensional homogeneous formulation of the governing equations for boiling flow in a horizontal tube. The results demonstrate the ability of the method to handle flow across the saturation lines, even when the initial crossing is at a boundary. To our knowledge, this has not been demonstrated elsewhere in the literature. A certain combination of numerical boundary conditions demonstrates both stability and conservation of mass, even in dynamic simulations with rapidly changing boundary conditions. While mass must be conserved, it is certainly not trivial to guarantee in a local numerical scheme, since mass is an integrated quantity. The method is also found to be easily parallelizable using a high level language like OpenMP.

References

[1] X.D. He, S. Liu, H. Asada, and H. Itoh, Multivariable control of vapor compression systems, HVAC&R Research, 4, 205-230, 1998.

[2] M. Willatzen, N.B.O.L. Pettit, and L. Ploug-Sørensen, A general simulation model for evaporators and condensers in refrigeration. Part I: Moving boundary formulation of two-phase flows with heat exchange, Int. J. Refrig., 21, 398-403, 1998.

[3] W.-J. Zhang, C.-L. Zhang, A generalized moving-boundary model for transient simulation of dry-expansion evaporators under larger disturbances, Int. J. Refrig., 29, 1119-1127, 2006.

[4] T. L. McKinley, A. G. Alleyne, An advanced nonlinear switched heat exchanger model for vapor compression cycles using the moving-boundary method, Int. J. Refrig., 31, 1253-1264, 2008.
[5] S .Madsen, C.T. Veje and M. Willatzen, Implementation Of The Kurganov-Tadmor High Resolution Semi-Discrete Central Scheme For Numerical Solution Of The Evaporation Process In Dry Expansion Evaporators, in Proceedings of the 50'th SIMS Conference, 2009.
[6] X. Jia, C.P. Tso, P.K. Chia and P. Jolly, A distributed model for prediction of the transient response of an evaporator, Int. J. Refrig., 18, 336-342, 1995.
[7] X. Jia, C.P. Tso, P. Jolly and Y.W. Wong, Distributed steady and dynamic modeling of dry-expansion evaporators, Int. J. Refrig., 22, 126-136, 1999.
[8] O. Garcia-Valladares, C.D. Perez-Segarra and J. Rigola, Numerical simulation of double-pipe condensers and evaporators, Int. J. Refrig., 27, 173-182, 2004.
[9] S. Morales-Ruiz, J. Rigola, C.D. Perez-Segarra, O. Garcia-Valladares, Numerical analysis of two-phase flow in condensers and evaporators with special emphasis on single-phase/two-phase transition zones, Appl. Therm. Eng., 29, 1032-1042, 2009.
[10] A. Kurganov, E. Tadmor, New high-resolution semi-discrete central schemes for Hamilton-Jacobi equations, Journal of Computational Physics, 160, 720-742, 2000.
[11] A. Kurganov, E. Tadmor, New high-resolution central schemes for nonlinear conservation laws and convection-duiffusion equations, Journal of Computational Physics, 160, 241-282, 2000.
[12] S. Karni, E. Kirr, A. Kurganov, and G. Petrova, Compressible two-phase flows by central and upwind schemes, ESIAM: Math. Model. and Num. Anal., 38, 477-493, 2004.
[13] S. Mostafa Ghiaasiaan, Two-Phase Flow, Boiling, and Condensation: In Conventional and Miniature Systems, Cambridge University Press, 1st edition, October 22, 2007.
[14] Lemmon, E.W., Huber, M.L., McLinden, M.O. NIST Standard Reference Database 23: Reference Fluid Thermodynamic and Transport Properties-REFPROP, Version 9.0, National Institute of Standards and Technology, Standard Reference Data Program, Gaithersburg, 2010.
[15] G. Wallis, One-dimensional Two-phase Flow, McGraw-Hill, 1969.
[16] John G. Collier and John R. Thome, Convective Boiling and Condensation, 3rd Edition, Oxford University Press, 198 Madison Avenue, New York, 1996.
[17] R. E. Carlson and F. N. Fritsch, An Algorithm For Monotone Piecewise Bicubic Interpolation, SIAM J. Numer. Anal., 26, No. 1, 230-238, 1989.
[18] S. Gottlieb, On High Order Strong Stability Preserving Runge-Kutta and Multi Step Time Discretizations, J. Sci. Comput., 25, 105-128, 2005.
[19] D. Buecker and W. Wagner, Reference Equations of State for the Thermodynamic Properties of Fluid Phase n-Butane and Isobutane, J. Phys. Chem. Ref. Data, 35(2), 929-1019, 2006.